Detection of Micrometastases Using SPECT/Fluorescence Dual-Modality Imaging in a CEA-Expressing Tumor Model

Marlène C.H. Hekman[1,2], Mark Rijpkema[1], Desirée L. Bos[1], Egbert Oosterwijk[2], David M. Goldenberg[3], Peter F.A. Mulders[2], and Otto C. Boerman[1]

[1]Department of Radiology and Nuclear Medicine, Radboud University Medical Center, Nijmegen, The Netherlands; [2]Department of Urology, Radboud University Medical Center, Nijmegen, The Netherlands; and [3]Immunomedics, Inc., Morris Plains, New Jersey

Intraoperative dual-modality imaging can help the surgeon distinguish tumor from normal tissue. This technique may prove particularly valuable if small tumors need to be removed that are difficult to detect with the naked eye. The humanized anticarcinoembryonic antigen (anti-CEA) monoclonal antibody, labetuzumab, can be used as a tumor-targeting agent in colorectal cancer, since CEA is overexpressed in approximately 95% of colorectal cancer. Dual-labeled labetuzumab, labeled with both a near-infrared fluorescent dye (IRDye800CW) and a radioactive label (^{111}In), can be used as a tracer for dual-modality imaging. This study aimed to assess whether dual-modality imaging using ^{111}In-diethylenetriaminepentaacetic acid (DTPA)–labetuzumab-IRDye800CW can detect pulmonary micrometastases in a mouse model. **Methods:** Pulmonary GW-39 human colonic carcinoma microcolonies were induced in athymic BALB/c mice by intravenous injection of 100 μL of a GW-39 cell suspension. After 1, 2, 3, and 4 wk of tumor growth, dual-modality imaging was performed 3 d after intravenous injection of ^{111}In-DTPA-labetuzumab-IRDye800CW (10 μg, 25 MBq). Small-animal SPECT images and optical images were acquired, and image-guided surgery was performed. Finally, the biodistribution of the dual-labeled tracer was determined. Formalin-fixed sections of the lungs were analyzed using fluorescence imaging, autoradiography, and immunohistochemistry. **Results:** Submillimeter pulmonary tumor colonies could be visualized with both small-animal SPECT and fluorescence imaging from the first week of tumor growth, before they became visible to the naked eye. Furthermore, dual-modality imaging could be used to guide resection of tumors. Mean uptake (percentage injected dose per gram) of the dual-labeled tracer in tumors was 17.2 ± 5.4 and 16.5 ± 4.4 at weeks 3 and 4, respectively. Immunohistochemical analysis of the tumorous lungs showed that the distribution of the radioactive and fluorescent signal colocalized with CEA-expressing tumors. **Conclusion:** Dual-modality imaging after injection of ^{111}In-labetuzumab-IRDye800CW can be used to detect submillimeter CEA-expressing pulmonary tumors before they become visible to the naked eye, supporting the added value of this technique in the resection of small tumors.

Key Words: molecular imaging; colorectal cancer; CEA; labetuzumab; fluorescence-guided surgery

Radical tumor resection is crucial to optimize the prognosis of cancer patients (1–6). However, during surgery small tumors or positive surgical margins can be difficult to detect with the naked eye. Sensitive intraoperative imaging techniques could help the surgeon visualize these small tumors that otherwise might be missed. Targeted dual-modality image-guided surgery using monoclonal antibodies tagged with both a fluorescent and a radioactive label combines the advantages of radioguided and fluorescence-guided surgery (7–14). The monoclonal antibody ensures adequate targeting of a tumor-associated antigen. The radioactive label allows localization of both deep and superficial tumors, whereas the fluorescent label enables the surgeon to visualize, delineate, and resect the tumors with fluorescence-guided surgery.

Labetuzumab is a humanized monoclonal antibody that specifically recognizes carcinoembryonic antigen (CEA), which is overexpressed in approximately 95% of colorectal cancer (15). CEA is considered to be the preferred biomarker for in vivo targeting of colorectal cancer (15). In colorectal cancer, incomplete tumor resection has a clearly negative effect on prognosis (16). A special surgical challenge are those patients with multiple small metastases limited to the peritoneal cavity (peritoneal carcinomatosis). In these patients, long-term control of disease can be achieved by cytoreductive surgery (resection of all visible tumor tissue) in combination with hyperthermic intraperitoneal chemotherapy (17–21). However, the presence of tumor residue after cytoreduction negatively affects prognosis (18,20,21). Intraoperative imaging can help the surgeon limit residual disease. Rijpkema et al. have shown the feasibility of image-guided surgery with ^{111}In-labetuzumab-IRDye800CW in mice with intraperitoneal, CEA-positive LS174T tumors (14). However, to be of optimal benefit in the operating room, dual-modality imaging should be able to detect very small tumors that can be missed with the naked eye.

The aim of the current study was to assess the feasibility of using dual-modality imaging with ^{111}In-labetuzumab-IRDye800CW to detect CEA-expressing pulmonary micrometastases. In this study, micrometastases were defined as tumors smaller than 2 mm according to the sixth edition of the *American Joint Committee on Cancer Staging Manual* for breast cancer (22). For this aim, a model with CEA-expressing pulmonary tumors was used, since it is an optimal model to study micrometastatic disease (23).

MATERIALS AND METHODS

Animal Model and Tumor Induction

All animal studies were approved by the institutional Animal Welfare Committee of the Radboud University Medical Center, and experiments were conducted in accordance with the principles of the revised Dutch

Act on Animal Experimentation (WOD 2014). Twenty-eight female athymic BALB/c *nu/nu* mice (6–8 wk old; Janvier) were acclimatized to laboratory conditions for at least 1 wk before use. They were housed in individually ventilated cages with ad libitum access to food and water.

The CEA-expressing GW-39 cell line was obtained from Immunomedics, Inc. Subcutaneous GW-39 xenografts were grown to 1 cm^3 and serially transplanted in BALB/c *nu/nu* mice. Six mice were euthanized, and their tumors were harvested, cut into pieces, filtered through a 400-μm mesh, and resuspended to a 10% cell suspension in culture medium (Roswell Park Memorial Institute medium plus penicillin/streptomycin) while kept on ice to be used for the 28 mice in the experiment, as described by Sharkey et al. (*23*). The first 15 mice received 100 μL of this cell suspension intravenously with a 23-gauge needle to induce micrometastatic disease in the lungs. Three mice died during intravenous injection because of inadequate suspension of the tumor cells. Therefore, the cell suspension was filtered again through a 200-μm mesh. The remaining 13 of the 28 mice were injected with 100 μL of this cell suspension without experiencing any health problems.

Mice injected with different cell suspensions were equally distributed over the experimental groups. The cell concentration in both cell suspensions was counted by adding ZAP-OGLOBIN II lytic reagent (Beckman Coulter) to a sample, stirring in a vortex mixer, and moving the cells up and down through a 23-gauge needle. Subsequently, the nuclei were counted using a Bürker-Türk counting chamber. The cell suspensions before and after extra filtration contained 3.7 and 3.5 million cells per milliliter, respectively.

All animals developed pulmonary tumors. Animal health was monitored on a daily basis, and body weight was measured 3 times a week. Two weeks after injection of the tumor cells, 1 mouse had to be removed from the experiment prematurely because of dyspnea and weight loss originating from excessive pulmonary tumor growth. For the same reason, 1 animal from week 4 was scanned 2 d (instead of 3 d) after injection of the tracer. In total, 6, 7, 6, and 5 animals were used in the experiment at weeks 1, 2, 3, and 4, respectively.

Dual-Labeled Antibody Production

Humanized labetuzumab (IgG type 1) was kindly provided by Immunomedics Europe. The fluorophore IRDye800CW-NHS ester was purchased from LI-COR Biosciences. The bifunctional chelator *p*-isothiocyanatobenzyl (ITC)–diethylenetriaminepentaacetic acid (DTPA) was purchased from Macrocyclics. First, labetuzumab (10 mg/mL) was incubated in 0.1 M NaHCO$_3$, pH 8.5, with a 3-fold molar excess of the IRDye800CW-NHS ester (room temperature, 1 h). Then, the mixture was incubated in 0.1 M NaHCO$_3$, pH 9.5, with a 20-fold molar excess of the ITC-DTPA (room temperature, 1 h). To remove the unconjugated IRDye800CW and ITC-DTPA, the reaction mixture was transferred into a Slide-A-Lyzer cassette (molecular weight cutoff: 20,000 Da; Thermo Scientific) and extensively dialyzed against 0.25 M NH$_4$Ac, pH 5.5, for 3 d with buffer changes. The average substitution ratio of IRDye800CW molecules was 1.2/antibody as determined by an Ultrospec 2000 ultraviolet/visible spectrophotometer (Pharmacia Biotech). Since GW39 cells cannot be cultured in vitro, the immunoreactive fraction of dual-labeled labetuzumab was determined after 6 h of incubation with CEA-expressing LS174T cells, essentially as described by Lindmo et al. (*24*), and was 90%. DTPA-labetuzumab-IRDye800CW was stored in the dark at 4°C until use.

Radiolabeling of DTPA-Labetuzumab-IRDye800CW

DTPA-labetuzumab-IRDye800CW was incubated with 0.5 M 2-(*N*-morpholino)ethanesulfonic acid (30 min, room temperature) and ^{111}InCl$_3$ (Mallinckrodt Pharmaceuticals). Then, unincorporated ^{111}In was chelated by adding 50 mM ethylenediaminetetraacetic acid to a final concentration of 5 mM. Radiochemical purity was determined by instant thin-layer chromatography on silica gel strips, using 0.1 M

sodium citrate buffer, pH 6.0, as the mobile phase. Radiochemical purity always exceeded 95%. Standards of the injected dose were prepared in triplicate to allow quantification of antibody accumulation, corrected for radioactive decay for biodistribution studies.

Dual-Modality Imaging

Groups of mice were injected via the tail vein with ^{111}In-labetuzumab-IRDye800CW (10 μg, 25 MBq of ^{111}In) (7 mice per time point). Three days later (after 1, 2, 3, or 4 wk of tumor growth), dual-modality imaging was performed. First, the mice were euthanized using O$_2$/CO$_2$ and the lungs were fixed by intratracheal injection of 4% formalin with a 21-gauge needle. Then, small-animal SPECT/CT images were obtained by scanning supine mice with a U-SPECT II (MILabs), using a 1.0-mm-diameter multipinhole ultra-high-sensitivity mouse collimator tube. The total scanning time was 50 min per animal (2 time frames, 24 bed positions, fast scan mode) for SPECT acquisitions and 3 min for CT acquisitions. Subsequently, the thoracoabdominal wall was removed surgically, and the mice were placed supine in an IVIS Lumina (Caliper Life Sciences) closed-cabinet fluorescence scanner (recording time, 1–5 min; binning factor, small or medium; F/stop, 2–4; excitation filter, 745 nm; emission filter, indocyanine green; field of view, C; autofluorescence [675 nm]; and background correction). Fluorescence imaging was performed before and after resection of tumors. Thereafter, the lungs were resected and scanned ex vivo in the closed-cabinet fluorescence scanner (field of view, A) and with an Odyssey CLx (LI-COR Biosciences) flatbed fluorescence scanner (recording time, ±5 min; channel, 800 nm; focus, 1.0 mm).

Biodistribution

After dual-modality imaging, the biodistribution of the radiolabel was determined: blood, muscle, heart, spleen, kidney, pancreas, liver, stomach, duodenum, and tumors were resected and weighed, and the amount of ^{111}In in these tissues was determined in a γ-counter (2480 WIZARD^2; Perkin Elmer). To correct for radioactive decay, samples were measured along with standards of the injected dose (in triplicate). The organ accumulation of ^{111}In-DTPA-labetuzumab-IRDye800CW was expressed as percentage injected dose per gram of tissue (%ID/g). Values are represented as mean uptake ± SD. Statistical analyses were performed using SPSS Statistics 22.0 (IBM). Tissue uptake at the different time points was tested for significance using a 1-way ANOVA test with post hoc Bonferroni adjustments. An α-value of 0.05 was used in all analyses.

Immunohistochemical Analysis

Formalin-fixed, paraffin-embedded, 5-μm sections of the lungs were cut and analyzed autoradiographically after 1.5 wk of exposure to a phosphor imaging plate. This plate was developed using the Typhoon FLA 7000 (GE Healthcare) phosphor imager and analyzed with Aida Image Analyzer, version 4.21 (Raytest). Next, fluorescence imaging of the pulmonary sections was performed with the flatbed fluorescence scanner (channel, 800 nm; recording time, 1–5 min; focus, 1.0 mm). Subsequently, sections were stained for CEA with humanized labetuzumab, as described previously by Schoffelen et al. (*25*), and counterstained with hematoxylin. On adjacent tissue sections, standard hematoxylin and eosin staining was performed.

RESULTS

Dual-Modality Imaging

Submillimeter pulmonary tumors could be visualized with dual-modality imaging in all animals that were imaged from the first week of tumor growth onward (Fig. 1 and Supplemental Fig. 1; supplemental materials are available at http://jnm.snmjournals. org). Small-animal SPECT/CT showed uptake of dual-labeled labetuzumab in pulmonary tumors and limited uptake in the liver,
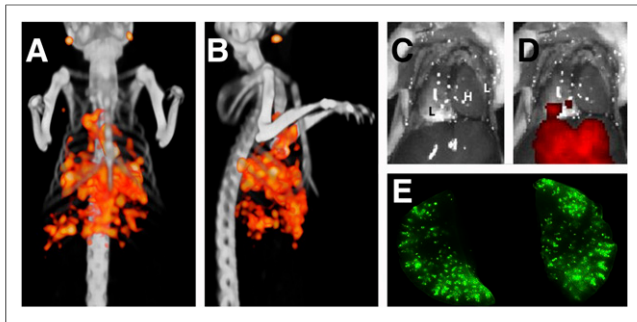
FIGURE 1. Example of dual-modality imaging in mouse 1 wk after tumor cell injection. (A and B) Pulmonary tumors could be seen with small-animal SPECT/CT on coronal (A) and sagittal (B) views. Some physiologic uptake of tracer in liver and lymph nodes was observed. (C) After resection of thoracoabdominal wall, no tumors were visible to the naked eye. (D) Imaging with closed-cabinet fluorescence scanner showed superficial tumors. (E) Imaging of resected lungs with flatbed fluorescence scanner showed numerous pulmonary lesions. L = lung; H = heart.

spleen, and lymph nodes (Figs. 1A and 1B). After resection of the thoracoabdominal wall, no tumors were visible to the naked eye after 1 wk of tumor growth (Fig. 1C). However, superficial tumors smaller than 1 mm were identified with fluorescence imaging (Figs. 1D and 1E). The presence of these CEA-expressing tumors was confirmed by immunohistochemistry, and the distribution of the radioactive and fluorescent signals in tissue sections (autoradiography and flatbed fluorescence imaging) colocalized with CEA-expressing tumors (Fig. 2; Supplemental Figs. 2 and 3). Pulmonary tumors became visible by macroscopic inspection after 2 wk of tumor growth. However, CEA-targeted dual-modality imaging revealed additional pulmonary tumors that had been missed by macroscopic inspection (Supplemental Fig. 4). No metastases were seen outside the lungs. After 3 or 4 wk of tumor growth, tumors were clearly visible to the naked eye and were visualized by dual-modality imaging.

Fluorescence-Guided Surgery

Superficial pulmonary lesions identified with fluorescence imaging were subsequently resected on the basis of their fluorescent signal. In the example shown in Figure 3 and Supplemental Figure 5 (3 wk after tumor induction), the lungs were imaged again after resection of the tumors to confirm that a radical tumor resection had been performed (Figs. 3B and 3D). Autoradiography of the tissue sections and immunohistochemistry did not identify remaining tumors (Fig. 3E).

Biodistribution

One and 2 wk after tumor induction, quantification of tumor uptake was unreliable because the tumor weight could not be determined accurately. At weeks 3 and 4, mean uptake of the dual-labeled tracer in tumors was 17.2 ± 5.4 %ID/g and 16.5 ± 4.4 %ID/g, respectively. Blood levels of the dual-labeled tracer decreased from 16.5 ± 2.8 %ID/g in the group imaged 1 wk after tumor induction to 7.7 ± 1.3 %ID/g in the group imaged 4 wk after tumor induction. Tracer uptake in the other organs is shown in Figure 4 and Supplemental Table 1. Apart from the liver, uptake in all organs was significantly lower at week 4 than at week 1.

DISCUSSION

This study showed the potential of CEA-targeted dual-modality imaging using dual-labeled labetuzumab to detect CEA-expressing

micrometastases before they become visible to the naked eye. Furthermore, the study showed that dual-labeled labetuzumab can be used to perform image-guided surgery on very small tumors. These results support the added value of dual-modality imaging in the visualization and resection of small tumors.

Labetuzumab is a humanized monoclonal antibody that specifically recognizes CEA. Clinical studies have shown the potential of radiolabeled anti-CEA antibodies for SPECT imaging and radioimmunotherapy, but imaging-guided surgery with dual-labeled labetuzumab still awaits clinical translation (*26,27*). In a previous study, we showed the feasibility of image-guided surgery with ^{111}In-labetuzumab-IRDye800CW in mice with intraperitoneal CEA-positive LS174T tumors (*14*). In the current study, we showed the added value of dual-modality imaging by assessing the feasibility of detecting micrometastases. For this purpose, the GW-39 model was chosen, since it is a well-established colorectal cancer model for studying CEA-expressing micrometastatic disease in the lungs (*23*). The finding that dual-modality imaging can detect micrometastatic disease is promising. Although the role for surgery in pulmonary metastases of colorectal cancer origin is limited, the current results could also apply to other CEA-expressing cancers or, when using a different tumor-targeting agent, to other types of cancer; for example, dual-labeled farletuzumab (antifolate receptor-α) in ovarian cancer surgery. The main role for surgery in metastasized colorectal cancer is in patients with metastases that are limited to the peritoneal cavity and in a subgroup of patients with limited liver metastases. Patients with peritoneal carcinomatosis represent a specific surgical challenge because lesions can be very small, numerous, and difficult to differentiate from scar tissue after previous surgery. In this study, we demonstrated that CEA-expressing micrometastases can be detected sensitively with the dual-modality imaging agent. In peritoneal carcinomatosis, tumors are located superficially on the abdominal organs instead of being distributed within a solid organ, such as in our pulmonary
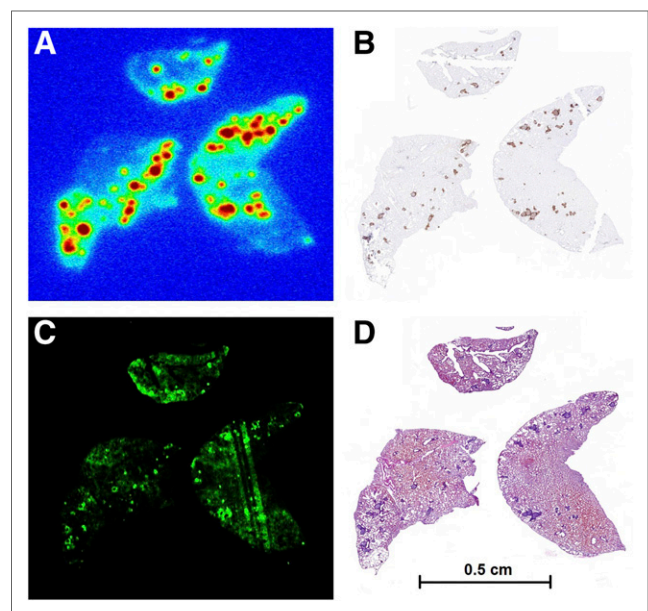

FIGURE 2. Autoradiography (A), fluorescence imaging (C), and immunohistochemistry (CEA [B] and hematoxylin and eosin [D]) of 5-μm paraffin-embedded pulmonary sections confirmed presence of submillimeter tumors in lungs after 1 wk of tumor growth. Fluorescent and radioactive signals colocalized with CEA-expressing tumors.
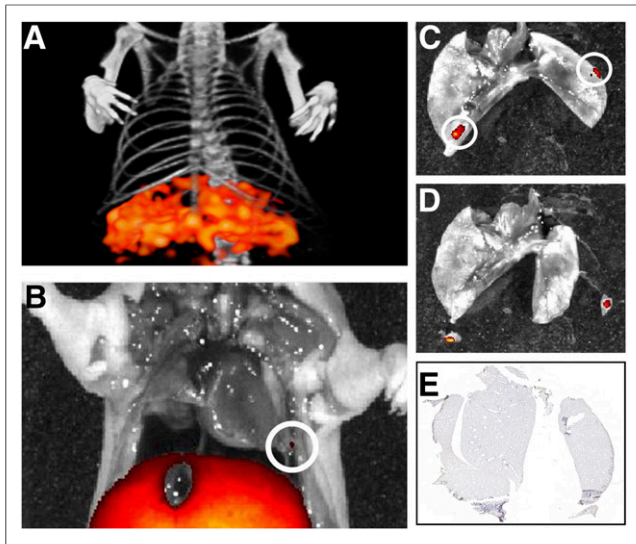
FIGURE 3. Example of image-guided surgery using dual-labeled labetuzumab at week 3. (A) Small-animal SPECT/CT did not reveal any pulmonary lesion, probably because lesions were near liver. (B) Fluorescence imaging revealed a superficial pulmonary nodule. (C) Fluorescence imaging of resected lungs revealed a second nodule behind lung. (D) Both lesions were resected using fluorescence-guided surgery. (E) CEA staining of lung sections did not reveal any remaining lesions.

model. Together with the mobility of the intraabdominal organs (e.g., intestines), this superficial location may simplify the use of dual-modality imaging in the abdominal setting compared with the pulmonary setting. The high liver uptake of ^{111}In-labetuzumab-IRDye800CW and the prolonged retention of ^{111}In in the liver may limit the role of the dual-labeled agent in the detection of micrometastases in or near the liver. Clinical trials with ^{111}In-labeled antibodies in other tumor types have shown that imaging of liver metastases with ^{111}In-labeled monoclonal antibodies is feasible (28,29). However, the addition of a fluorescent label (IRDye800CW) may reduce tumor-to-liver contrast because of the enhanced uptake in the liver (30). Therefore, dual-modality imaging using ^{111}In-labetuzumab-IRDye800CW may not be useful for intraoperative detection of small liver metastases.
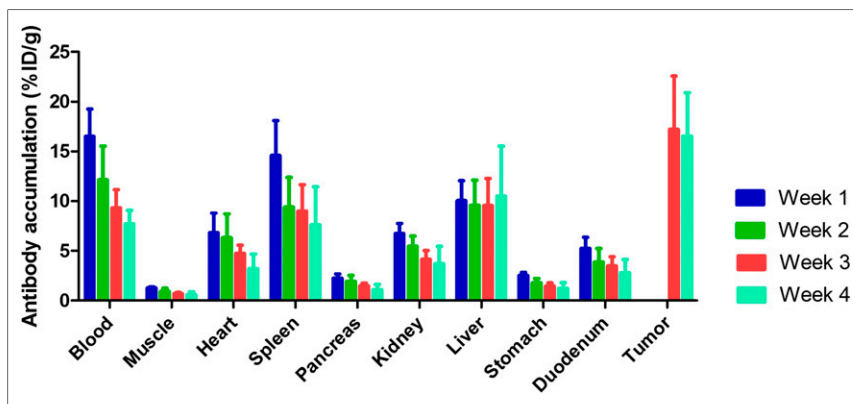
FIGURE 4. Biodistribution of ^{111}In-DTPA-labetuzumab-IRDye800CW at 72 h after injection at 1, 2, 3, and 4 wk after tumor induction. One and 2 weeks after tumor induction, tumors were too small for reliable quantification, since tumor weight could not be determined accurately. Apart from liver, uptake in all organs was significantly lower at week 4 than at week 1. Tissue uptake is expressed as % ID/g. Values represent mean ± SD.

In the current study, submillimeter pulmonary tumor colonies could be visualized with dual-modality imaging before they became visible to the naked eye. Image-guided resection of tumors was performed after 3 and 4 wk of tumor growth. Figure 3 demonstrates that dual-modality imaging can be used to check whether a tumor has been completely resected. Because most of the mice had numerous pulmonary tumors, resection of all tumors was challenging in this model. Biodistribution studies showed that the mean uptake of dual-labeled labetuzumab in tumors was 17.2 ± 5.4 %ID/g and 16.5 ± 4.4 %ID/g at weeks 3 and 4, respectively. Mean blood levels of dual-labeled labetuzumab decreased gradually from week 1 to week 4 after tumor induction (16.5, 12.1, 9.3, and 7.7 %ID/g at weeks 1, 2, 3, and 4, respectively). An explanation might be that in mice with a higher tumor load, there is increased shedding of CEA from tumors into the blood and therefore faster clearance of the dual-labeled antibody, as was described previously (31,32). Sharkey et al. reported that there is significant complexation of the antibody in the presence of high plasma CEA levels (>400 ng/mL) and that patients with elevated CEA levels have faster blood clearance of radiolabeled labetuzumab (33). Complexation could be reduced by increasing the protein dose (33). This phenomenon has to be considered when applying CEA-targeted imaging with dual-labeled labetuzumab in patients. An alternative is to exclude patients with very high plasma CEA levels.

The advantage of a dual-labeled tracer is that the same tracer can be used for preoperative and intraoperative imaging. Preoperative CT or ^{18}F-FDG PET fail to detect peritoneal carcinomatosis in approximately 9% and 17% of patients, respectively (34). ^{111}In-labetuzumab-IRDye800CW SPECT/CT might be used to detect colorectal cancer metastases preoperatively. Tumors can be localized intraoperatively with a γ-probe, and a fluorescence camera can subsequently be used to guide and facilitate tumor resection and assess the surgical cavity for remnant disease. That both techniques are complementary to each other is illustrated in Figures 1 and 3. Because of the limited penetration of light, only superficial tumors can be detected with fluorescence imaging (Figs. 1D, 1E, 3B, and 3C). However, preoperative SPECT/CT reveals that the tumor load is more extensive (Figs. 1A and 1B), and in humans, a γ-probe can be used together with a fluorescence camera for intraoperative tumor detection. The dual-labeled approach ensures that both signals originate from the same molecule, in contrast to coinjection of a radiolabeled and a fluorescently labeled agent.

Although this study demonstrated the feasibility of dual-modality imaging of very small CEA-expressing tumors, there are some limitations that have to be considered. Because imaging was performed on euthanized animals, direct translation of these results to humans is premature. Also, one should consider that the sensitivity of real-time fluorescence imaging scanners used in the clinic differs significantly from the scanners that were used in this study. Several reports have shown the feasibility of targeted fluorescence imaging of cancer in humans (8,35,36); however, the technique is still in its infancy and has to be optimized before it can be used in clinical practice. Another consideration is that the spatial resolution of images acquired with clinical PET scanners is higher than the resolution of SPECT scanners. Therefore, for preoperative imaging

purposes, the use of a positron-emitting radionuclide—for example, ^{89}Zr—could be beneficial. However, the 511-keV γ-rays are less suitable for intraoperative detection with a standard γ-probe. Therefore, the optimal tracer depends on the clinical question.

CONCLUSION

This study showed the potential of CEA-targeted dual-modality imaging using dual-labeled labetuzumab to detect and resect CEA-expressing micrometastases. These data support the initiation of a feasibility study of dual-modality, image-guided surgery with ^{111}In-DTPA-labetuzumab-IRDye800CW in patients with peritoneal carcinomatosis of colorectal origin.

DISCLOSURE

David M. Goldenberg is an officer of Immunomedics and is an inventor on patents related to this technology. No other potential conflict of interest relevant to this article was reported.

REFERENCES

1. Borghesi M, Brunocilla E, Schiavina R, Martorana G. Positive surgical margins after nephron-sparing surgery for renal cell carcinoma: incidence, clinical impact, and management. *Clin Genitourin Cancer.* 2013;11:5–9.
2. Swindle P, Eastham JA, Ohori M, et al. Do margins matter? The prognostic significance of positive surgical margins in radical prostatectomy specimens. *J Urol.* 2008;179(suppl):S47–S51.
3. Meric F, Mirza NQ, Vlastos G, et al. Positive surgical margins and ipsilateral breast tumor recurrence predict disease-specific survival after breast-conserving therapy. *Cancer.* 2003;97:926–933.
4. Singletary SE. Surgical margins in patients with early-stage breast cancer treated with breast conservation therapy. *Am J Surg.* 2002;184:383–393.
5. Dotan ZA, Kavanagh K, Yossepowitch O, et al. Positive surgical margins in soft tissue following radical cystectomy for bladder cancer and cancer specific survival. *J Urol.* 2007;178:2308–2312.
6. Haque R, Contreras R, McNicoll MP, Eckberg EC, Petitti DB. Surgical margins and survival after head and neck cancer surgery. *BMC Ear Nose Throat Disord.* 2006;6:2.
7. Luker GD, Luker KE. Optical imaging: current applications and future directions. *J Nucl Med.* 2008;49:1–4.
8. van Dam GM, Themelis G, Crane LM, et al. Intraoperative tumor-specific fluorescence imaging in ovarian cancer by folate receptor-alpha targeting: first in-human results. *Nat Med.* 2011;17:1315–1319.
9. Vidal-Sicart S, van Leeuwen FW, van den Berg NS, Valdes Olmos RA. Fluorescent radiocolloids: are hybrid tracers the future for lymphatic mapping? *Eur J Nucl Med Mol Imaging.* 2015;42:1627–1630.
10. Verbeek FP, Tummers QR, Rietbergen DD, et al. Sentinel lymph node biopsy in vulvar cancer using combined radioactive and fluorescence guidance. *Int J Gynecol Cancer.* 2015;25:1086–1093.
11. Lütje S, Rijpkema M, Franssen GM, et al. Dual-modality image-guided surgery of prostate cancer with a radiolabeled fluorescent anti-PSMA monoclonal antibody. *J Nucl Med.* 2014;55:995–1001.
12. Lütje S, Rijpkema M, Helfrich W, Oyen WJ, Boerman OC. Targeted radionuclide and fluorescence dual-modality imaging of cancer: preclinical advances and clinical translation. *Mol Imaging Biol.* 2014;16:747–755.
13. Muselaers CH, Rijpkema M, Bos DL, et al. Radionuclide and fluorescence imaging of clear cell renal cell carcinoma using dual labeled anti-carbonic anhydrase IX antibody G250. *J Urol.* 2015;194:532–538.
14. Rijpkema M, Oyen WJ, Bos D, Franssen GM, Goldenberg DM, Boerman OC. SPECT- and fluorescence image-guided surgery using a dual-labeled carcinoembryonic antigen-targeting antibody. *J Nucl Med.* 2014;55:1519–1524.
15. Tiernan JP, Perry SL, Verghese ET, et al. Carcinoembryonic antigen is the preferred biomarker for in vivo colorectal cancer targeting. *Br J Cancer.* 2013;108:662–667.
16. Gravante G, Hemingway D, Stephenson JA, et al. Rectal cancers with microscopic circumferential resection margin involvement (R1 resections): survivals, patterns of recurrence, and prognostic factors. *J Surg Oncol.* 2016;114:642–648.
17. Verwaal VJ. Cytoreduction and HIPEC for peritoneal carcinomatosis from colorectal origin: the Amsterdam experience. *Acta Chir Belg.* 2006;106: 283–284.
18. Verwaal VJ, Boot H, Aleman BM, van Tinteren H, Zoetmulder FA. Recurrences after peritoneal carcinomatosis of colorectal origin treated by cytoreduction and hyperthermic intraperitoneal chemotherapy: location, treatment, and outcome. *Ann Surg Oncol.* 2004;11:375–379.
19. Verwaal VJ, Bruin S, Boot H, van Slooten G, van Tinteren H. 8-year follow-up of randomized trial: cytoreduction and hyperthermic intraperitoneal chemotherapy versus systemic chemotherapy in patients with peritoneal carcinomatosis of colorectal cancer. *Ann Surg Oncol.* 2008;15:2426–2432.
20. Verwaal VJ, van Ruth S, de Bree E, et al. Randomized trial of cytoreduction and hyperthermic intraperitoneal chemotherapy versus systemic chemotherapy and palliative surgery in patients with peritoneal carcinomatosis of colorectal cancer. *J Clin Oncol.* 2003;21:3737–3743.
21. Verwaal VJ, van Tinteren H, van Ruth S, Zoetmulder FA. Predicting the survival of patients with peritoneal carcinomatosis of colorectal origin treated by aggressive cytoreduction and hyperthermic intraperitoneal chemotherapy. *Br J Surg.* 2004;91:739–746.
22. Green FL, Page DL, Fleming ID. *AJCC Cancer Staging Manual.* 6th ed. Chicago, IL: American Joint Commission on Cancer; 2002.
23. Sharkey RM, Karacay H, Vallabhajosula S, et al. Metastatic human colonic carcinoma: molecular imaging with pretargeted SPECT and PET in a mouse model. *Radiology.* 2008;246:497–507.
24. Lindmo T, Boven E, Cuttitta F, Fedorko J, Bunn PA Jr. Determination of the immunoreactive fraction of radiolabeled monoclonal antibodies by linear extrapolation to binding at infinite antigen excess. *J Immunol Methods.* 1984;72:77–89.
25. Schoffelen R, van der Graaf WT, Sharkey RM, et al. Pretargeted immuno-PET of CEA-expressing intraperitoneal human colonic tumor xenografts: a new sensitive detection method. *EJNMMI Res.* 2012;2:5.
26. Hajjar G, Sharkey RM, Burton J, et al. Phase I radioimmunotherapy trial with iodine-131-labeled humanized MN-14 anti-carcinoembryonic antigen monoclonal antibody in patients with metastatic gastrointestinal and colorectal cancer. *Clin Colorectal Cancer.* 2002;2:31–42.
27. Artiko V, Petrovic M, Sobic-Saranovic D, et al. Radioimmunoscintigraphy of colorectal carcinomas with ^{99m}Tc-labelled antibodies. *Hepatogastroenterology.* 2011;58:347–351.
28. Muselaers CH, Boerman OC, Oosterwijk E, Langenhuijsen JF, Oyen WJ, Mulders PF. Indium-111-labeled girentuximab immunoSPECT as a diagnostic tool in clear cell renal cell carcinoma. *Eur Urol.* 2013;63:1101–1106.
29. Pandit-Taskar N, O'Donoghue JA, Divgi CR, et al. Indium 111-labeled J591 anti-PSMA antibody for vascular targeted imaging in progressive solid tumors. *EJNMMI Res.* 2015;5:28.
30. Rijpkema M, Bos DL, Cornelissen AS, et al. Optimization of dual-labeled antibodies for targeted intraoperative imaging of tumors. *Mol Imaging.* 2015;14: 348–355.
31. Primus FJ, Wang RH, Cohen E, Hansen HJ, Goldenberg DM. Antibody to carcinoembryonic antigen in hamsters bearing GW-39 human tumors. *Cancer Res.* 1976;36:2176–2181.
32. Munjal D, Goldenberg DM. Carcinoembryonic antigen and glucose phosphate isomerase in a human colonic cancer model (GW-39). *Br J Cancer.* 1976;34:227–232.
33. Sharkey RM, Juweid M, Shevitz J, et al. Evaluation of a complementarity-determining region-grafted (humanized) anti-carcinoembryonic antigen monoclonal antibody in preclinical and clinical studies. *Cancer Res.* 1995;55:5935s–5945s.
34. Pasqual EM, Bertozzi S, Bacchetti S, et al. Preoperative assessment of peritoneal carcinomatosis in patients undergoing hyperthermic intraperitoneal chemotherapy following cytoreductive surgery. *Anticancer Res.* 2014;34:2363–2368.
35. Burggraaf J, Kamerling IM, Gordon PB, et al. Detection of colorectal polyps in humans using an intravenously administered fluorescent peptide targeted against c-Met. *Nat Med.* 2015;21:955–961.
36. Okusanya OT, DeJesus EM, Jiang JX, et al. Intraoperative molecular imaging can identify lung adenocarcinomas during pulmonary resection. *J Thorac Cardiovasc Surg.* 2015;150:28.e1–35.e1.